



Thermal, Fire, and Mechanical Properties of Solvent-Free Processed BN/Boehmite-Filled Prepregs

Christin Pawelski-Hoell , Sagar Bhagwat, Volker Altstädt

Department of Polymer Engineering, University of Bayreuth, Germany

Within the scope of this research, platelet-shaped hexagonal Boron Nitride (*h*-BN) with a size of 2 and 12 μm , and oval-shaped Boehmite (BT) with a size of 2 μm were incorporated in a glass fiber-reinforced epoxy novolac matrix cured with a diamine-based hardener. The effects of the platelet size (BN 2 and 12 μm) and filler nature (BT vs. BN) were correlated with the final thermal and fire-related properties. The incorporation of the fillers shows that not only the thermal conductivity (σ) was increased from approximately 0.2 up to 1.04 W/mK (through-plane) but also the flame retardancy was improved by using a hybrid combination. The time to ignition (t_{ig}) was increased by 48 s and the FIGRA value was decreased from 6.5 to 3.3 indicating a much lower fire hazard for the material. Scanning electron microscopic micrographs of the laminate cross sections show that the fillers are distributed and oriented randomly in the fiber-reinforced matrix, and also highlight the fiber wetting. Furthermore, the results show that the resulting 3D filler network and infiltration of the intratow regions is strongly dependent on lateral filler size and filler combination. With increasing the filler aspect ratio, the effect on thermal properties and filtration is more evident. Moreover, the hybrid combination of BN and Boehmite fillers has a strong effect on the network formation during processing, resulting in enhanced thermal and mechanical properties. A synergy was observed when using BN 12 μm in combination with Boehmite 2 μm as the larger platelets tend to assemble themselves in the intertow region (resin-rich region) and the smaller particles infiltrate into the intratow regions. This leads to a formation of a thermal pathway throughout the glass fabric barrier. Considering the cost factor, the through-plane (*z*-direction) heat dissipation and the flame retardancy can be tailored by optimizing the size, aspect ratio/geometry, and nature of the fillers. POLYM. ENG. SCI., 59:1840–1852, 2019. © 2019 The Authors. *Polymer Engineering & Science* published by Wiley Periodicals, Inc. on behalf of Society of Plastics Engineers.

INTRODUCTION

Current technological trends in electronics toward miniaturization, higher service temperatures, and dense switching powers have opened up critical thermal management issues. Early material failure due to the low heat spreading often occurs as delamination in the interlayer between the polymeric matrix (insulator) and the metallic-based assembly parts (highly thermally conductive). In the literature, it is well known that incorporating ceramic fillers

(i.e., AlN, BN, or Silica) with high intrinsic thermal conductivity (TC) increases the overall epoxy resins' thermal transport behavior [1, 2]. Many composite-based studies show that the filler size [3–9], geometry [4, 6, 10], concentration [3–9], and the fillers aspect ratio [11] play a crucial role for the 3D network formation of the fillers in order to build up a continuous channel for heat passing through. Moreover, the TC can be further enhanced by the combination of two fillers of different sizes [9, 10] and/or of different nature [5, 12]. Compared with the commonly known inorganic aluminum trihydroxide (=ATH), Boehmite (=AlO(OH)) is a promising candidate as it is thermally stable up to 350°C during printed circuit board (PCB) soldering or assembling processes. Furthermore, it offers a low CTE, offers good copper adhesion, and reduces the overall production costs of PCBs. Additionally, Boehmite is a halogen-free flame retardant (FR) with a TC in the range of 3–10 W/mK. Boehmite as an FR acts in both the gas and solid phases. The combustion process of polymers and the roles of the two phases are well explained in literature [13]. Boehmite decomposes in an endothermic reaction to solid Al₂O₃ by releasing water molecules, which cool down the burning system and interact with the ongoing free-radical reactions in the gas-phase. Additionally, the deposited Al₂O₃ acts as a thermal shield against heat and oxygen between the polymer and the flame in the so-called solid-phase [14].

With hexagonal Boron Nitride (*h*-BN) having an oval platelet shape, the thermal heat spreading is therefore more prominent in the planar level (300–600 W/mK), whereas in the perpendicular level, the TC is as low as 30 W/mK. A study by Yu et al. [15] shows that with the forced alignment through applied vacuum-filtration of platelet BN, the TC reaches values up to 9 W/mK with a 44 wt% loading in-plane. However, this procedure involves additional processing steps increasing the cycle time and only a 2D-heat transfer is resulting, whereas the targeted application of PCBs requires a 3D heat spread. Tsekmes et al. showed that with a filler concentration below 20 vol%, the TC of the matrix dominates. In addition, the authors demonstrated that a surface modification of fillers is only prevalent with decreasing filler size in nanometer range rather than affecting the TC in micrometer range [16]. Kochetov states that BN with a platelet geometry has a higher potential to increase the TC rather than a spherical-shaped BN. The filler distance of the platelets is much smaller as their aspect ratio is much higher, and therefore, the heat flow is enhanced [17].

Hill and Supancic studied the effect of different platelet-shaped fillers with different intrinsic thermal conductivities and found a correlation between the TC and the intrinsic filler hardness. Al₂O₃ or SiC are higher in their hardness than BN. BN, which is a filler of softer nature, can be deformed leading to a higher packing density, which directly leads to a higher TC [18]. Other applications of BN are in heat sink composites or adhesives. Hong et al. evaluated BN-containing polymer composites and the effect of adding metal particles and AlN. They reached a TC value of approximately 10 W/mK and studied the application of the BN/AlN combination for heat sinks [19]. The combination of micrometer-sized

Correspondence to: C. Pawelski-Hoell; e-mail: christin.pawelski@uni-bayreuth.de
Contract grant sponsor: Bundesministerium für Wirtschaft und Energie;
contract grant number: 0325916F.
DOI 10.1002/pen.25184

Published online in Wiley Online Library (wileyonlinelibrary.com).

© 2019 The Authors. *Polymer Engineering & Science* published by Wiley Periodicals, Inc. on behalf of Society of Plastics Engineers.

This is an open access article under the terms of the Creative Commons Attribution License, which permits use, distribution and reproduction in any medium, provided the original work is properly cited.

TABLE 1. Overview of the intrinsic physical filler properties.

Filler	Filler density (g/cm ³)	Particle size D ₅₀ (μm)	BET (m ² /g)	Shape	Aspect ratio	TC
AOH EXS (= BT)	3.07	2	4	Platelet	10	30
<i>h</i> -BN 410 (= BN 2 μm)	2.27	2	20	Platelet	16	30–300
<i>h</i> -BN 641 (=BN 12 μm)	2.35	12	7	Platelet	18	30–300

BN (0.5 μm) with nanosized Al₂O₃ (range of 20 nm up to 500 nm) in epoxy adhesives were studied by Fu et al. [20]. They found a synergy by the filler combination at 40 wt% in a ratio of 1:3 for TC, electrical insulation, and mechanical strength.

For being applicable in PCBs and being aligned with the thermal management trend, polymeric matrix materials with high thermal stability and T_g are of interest in the current state of the art. Epoxy resins can vary with a T_g between 160°C and 185°C, whereas epoxy novolac thermosets can reach glass transition temperatures from 180°C and above 200°C [21]. The incorporation of a glass fabric (GF) in PCBs is necessary in order to give structural stability and bending strength. With the processing of prepregs, a possible filtration and/or aggregation of the particles might occur due to the small gaps (intratow region) between the 0°/90°-GF tows. The incorporation of GF lowers the through-plane heat transport due to the filtration of the fillers and barrier effect of the fibers. However, there are very few studies on the relevance of processing, filtration effects, and the overall laminates' properties [22, 22, 23]. Devendra and Rangaswamy studied the effect of incorporating thermally conductive fillers in glass fiber-reinforced (GFRP) laminates. The authors observed that 10 vol% of SiC particles enhanced the TC of the laminates from 2.89 to 3.51 W/mK. They suggested the formation of a conductive pathway, which contributed to enhanced heat transfer [22]. A study by Fan et al. show the potential of introducing BN to a carbon-fiber-reinforced epoxy; 20 vol% of 1 μm BN leads to a TC of 7.9 W/mK. A proper morphological qualitative study that elaborates the structure–property relationship is missing [23]. In addition, compared with current industrial standard solvent-based impregnation, a new approach in technical scale is a complete solvent-free route. As the fillers increase the resins' viscosity tremendously, it is important to find the perfect interaction between the preparation of the formulation (mixing parameters, filler content, and their filler combinations) and the processing parameters (film coating speed and temperatures at the coating/heating unit).

Therefore, this study aims to scientifically understand the effect of a high filler content on the processing and impregnation behavior of epoxy novolac-based prepregs and their final properties. Furthermore, this study aims to correlate the effect of the microscale morphology with the macroscale final thermal properties, that is, TC T_g and flame retardancy.

TABLE 2. Overview of sample labeling and their relative ratio.

Sample labels	Filler composition	Relative ratio of fillers	Resin content (vol%, _{TGA})	Filler concentration (vol%, _{TGA})
Neat epoxy Novolac (DEN 438)	—	—	91.61	0.0
EP + BN 2 μm	Unimodal	—	72.54	15.65
EP + BN 12 μm	Unimodal	—	74.05	15.18
EP + BT 2 μm	Unimodal	—	78.61	12.73
EP + Boehmite 2 μm + BN 12 μm	Hybrid	1:3	76.84	14.01

All systems are filled with 40 wt% of fillers in the resin matrix.

EXPERIMENTAL

Materials and Preparation of Highly Filled Prepreg-Based EP-Novolac-GF Laminates

Materials. A multifunctional epoxy novolac resin, D.E.N.TM 438 from OlinTM Epoxy (Clayton) with an epoxy equivalent of 176–181 g/eq was used as a high T_g reference matrix resin, which was cured with diethymethylbenzenediamine (XB3473), supplied by Huntsman Advanced Chemicals (Basel, Switzerland), in the stoichiometric ratio of 100:24.1.

As an FR, Boehmite (oval shape), supplied by Nabaltec AG with a density of 3.07 g/cm³ and a D₅₀ of 2.0 μm, was used. Two *h*-BN types, purchased from Henze BNP with a D₅₀ of 2.0 and 12 μm, were used. All BN types are of platelet shape and have an average filler density between 2.27 and 2.35 g/cm³. The glass fabric (GF), with an areal weight of 25 g/m², United States style 106, was purchased from PD Interglas Technologies GmbH, Germany. The glass fibers are silane-coated to improve the adhesion to the epoxy novolac resin. The fiber bundles (warp/weft) are in plain-weave pattern. An overview of the physical properties of the used fillers and their labeling can be seen in Tables 1 and 2.

Resin Formulation. The mixing of the highly filled resin formulations was prepared as follows. To ensure even wetting and filler dispersion, the resin and the fillers were mixed at 200–250 rpm for 4 min so that the generated shear forces help in completely wetting the fillers. Later, the mixing speed was lowered to 180 rpm for about 15 min. After this, the hardener was incorporated, and the mixing speed was further lowered to 110 rpm to avoid excess generation of air inclusions. This formulation was then poured in the resin holding tank, which was maintained at a temperature of 80°C to avoid early gelation.

Prepreg Production. The completely solvent-free prepreg production was carried out on a lab-scale EHA Composites Machinery, Germany. The formulations were heated up to 85°C in the coating unit. The uncured resin formulations were then film-coated on a siliconized release paper using the direct coating method with a production speed of 1.5 m/min. The fabric was laid on the resin film and then covered with a second siliconized paper. The impregnation took

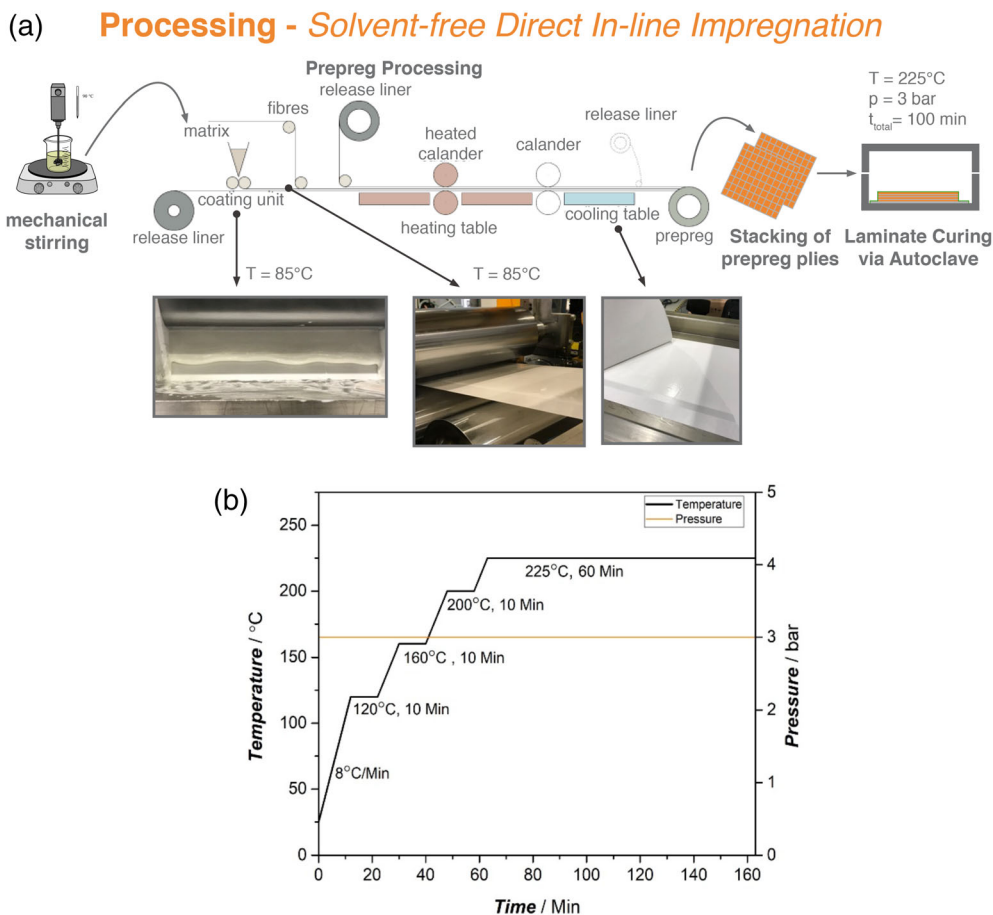


FIG. 1. (a) Schematic of the mixing, prepreg processing, and curing steps (autoclave setup) and (b) temperature/pressure curing profile for the processing of the GFRP-laminates. [Color figure can be viewed at wileyonlinelibrary.com]

place in the calendar unit at 85°C (Fig. 1a). The prepregs with a width of 200–220 mm were rolled up, sealed in a vacuum-bag, and kept at -18°C until further processing.

Prepreg-Based Laminate Production via Auto-Clave. The prepregs were cut into $200 \times 200 \text{ mm}^2$ single layers and roughly 32 layers were stacked up by hand layup on a steel plate and cured in an autoclave setup according to the curing cycle under vacuum ($< 25 \text{ mbar}$) and 3 bar air pressure (Fig. 1b). The detailed temperature–pressure profile can be seen in Fig. 1b. The final laminate thickness was $3 \text{ mm} \pm 0.15$.

Characterization Methods

TC measurements were carried out for the *through-plane* direction at a room temperature of 23°C using a heat flow meter FOX50 from TA Instruments (New Castle, United States) according to ASTM C518 in specimens with the diameter of 60 mm and a thickness of 3 mm. The specimens were subjected to grinding with SiC paper of the sizes 500, 1,200, and 2,000 μm and polished with a diamond suspension of particle sizes 6, 3, and 1 μm . Each sample was subjected to each SiC paper or diamond solution for 3 min with an applied 5 kN force and 150 rpm in anticlockwise direction. The accuracy of the Fox50 equipment is $\pm 3\%$ and the reproducibility is $\pm 2\%$.

The *through-* and *in-plane* measurements were carried out using the transient hot bridge (THB) method. The laminate samples were cut in half at the mid-section and were stacked together, once horizontally on top of each other (for *z*-plane) and once vertically (*x/y*-plane), with a highly temperature sensitive Kapton-sensor of placed in between. In addition, a weight of 5 kg (approximately 49 N) was placed on top on the sensor tip to ensure constant contact pressure on each sample.

Real-time *thermographic* images and time/temperature-profiles were detected with a VarioCam[®] hr from InfraTec, Germany. The specimens with a diameter of 60 mm were first subjected to a 80°C preheated isothermal hot plate and then cooled down to room temperature on a second hot plate setup. Both the heating and cooling rates were evaluated using the analysis software IRBIS[®] 3 professional [24].

Dynamic mechanical thermal analysis was performed at a heating rate of 3 K/min from 30°C to 280°C in torsional mode at an elastic

TABLE 3. Summarized properties of the produced laminates.

Specimen type	T_g ($^{\circ}\text{C}$)	FVC (vol%, _{TGA})	FVC (vol%, _{density})
Neat EP-novolac	235.4	8.39	19.0
EP + BN 2 μm	236.8	11.65	20.3
EP + BN 12 μm	237.7	10.77	20.5
EP + BT 2 μm	235.7	8.66	22.8
Hybrid	232.3	9.15	21.1

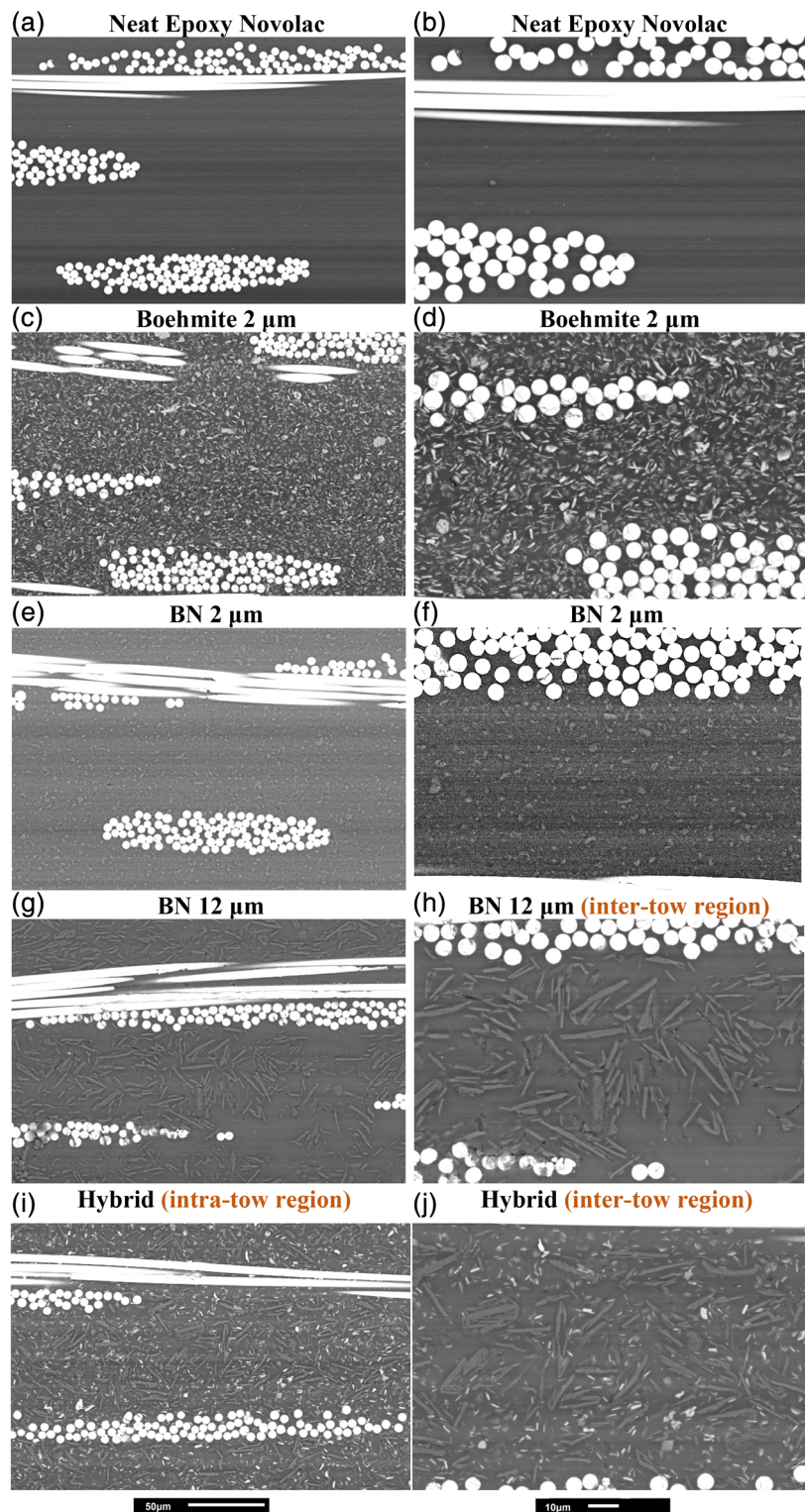


FIG. 2. SEM micrographs of the highly filled GFRP laminates in through-thickness indicating the filler dispersion, orientation, and eventual filtration for (a and b) neat epoxy novolac, (c and d) Boehmite 2 μm , (e and f) BN 2 μm , (g and h) BN 12 μm , and (i and j) hybrid combination (Boehmite 2 μm + BN 12 μm , ratio 1:3). The filler concentration is kept constant at 20 vol% in the resin film during GF impregnation. [Color figure can be viewed at wileyonlinelibrary.com]

deformation of 0.1% and an applied frequency of 1 Hz using the ARES RDA III from Rheometrics Scientific (Germany). The specimens had a rectangular geometry in a size of $50 \times 10 \times 2 \text{ mm}^3$ according to the standard DIN EN ISO 6721-7. The glass temperature

was evaluated using the maximum of the $\tan \delta$ curve with a standard deviation of temperature $\pm 0.375^\circ\text{C}$.

A cone calorimeter, iCONE™ FTT (UK) was used to evaluate the flame retardancy and other important fire properties, that is, t_{ig}

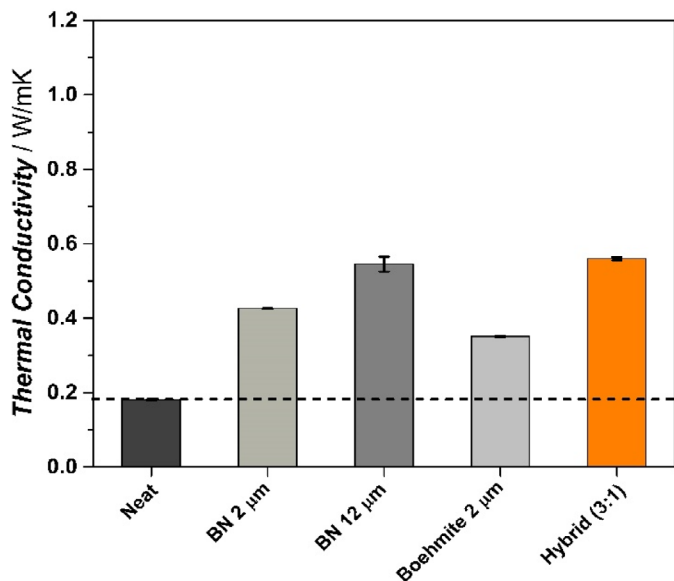


FIG. 3. TC measured with heat flow meter in through-thickness (z -plane) direction of the chosen GFRP laminates. (Hybrid = 20 vol% of three parts BN 12 μm and 1-part Boehmite 2 μm .) [Color figure can be viewed at wileyonlinelibrary.com]

(time to ignition), total smoke production (TSR), and heat release rate (HRR). The samples, with a geometry of $100 \times 100 \times 3\text{mm}^3$, were measured in a horizontal setup with an applied heat flux of 35 kW/m^2 and 23 mm distance between the sample and the cone heater. The FIGRA value is calculated by dividing peak heat release rate (PHRR) with the time to PHRR, which indicates the fire growth rate. Two samples of each composition were tested and averaged. The char residues were investigated as received after the cone calorimetric tests.

Scanning electron microscopic (SEM) measurements were obtained on a Jeol JSM 6510 instrument operating at 15 keV. Samples were embedded, polished, and then carbon-sputtered (thickness of coating: 20 nm). All micrographs are in backscatter electron composition mode.

Energy-dispersive X-ray spectroscopy (EDX) was used to study the combustion residues of the tested samples from the cone calorimetry test. These measurements were obtained on a Zeiss Leo 1530 instrument operating at 15 keV.

The fiber volume content (FVC) was determined via two different methods. The first method was via the density route according to the Archimedes principle by using a Mettler Toledo AG 245 analytical balance. The specimens were weighed in air and in water separately. Three samples of each system were measured and averaged. The standard deviation is $\rho \pm 0.038$.

The second method was via thermogravimetric analysis (TGA). The samples (15–20 mg) were heated from 25°C to 600°C under nitrogen atmosphere (50 mL/min) and from 600°C to 900°C in air (50 mL/min) at a heating rate of 10 K/min in order to access the fiber and filler residues. The standard deviation is $\text{mass} \pm 0.193$. The fiber and filler contents in wt% were calculated on the basis of the TGA residue masses and on the assumption that the ratio of fillers to resin is the same in the composite formulation and in the prepreg formulation. The vol% contents were calculated from the wt%; and the calculated densities from the TGA composition and on the densities of 2.57 g/cm^3 for

TABLE 4. Summary of achieved TC of the GFRP laminates as per method and measurement direction.

Specimen type	z -plane via hot plate	z -plane via THB	x/y plane via THB	Deviation z and x/y
Neat epoxy novolac	0.181	0.314	0.121	0.104
Boehmite 2 μm	0.359	0.473	0.338	0.135
BN 2 μm	0.426	0.605	0.425	0.180
BN 12 μm	0.545	1.043	0.665	0.378
Hybrid	0.560	0.831	0.615	0.216

BN 12 showed the highest TC values and the TC of the Hybrid combination was better than the unimodal BN2 and BT.

E-glass, 1.22 g/cm^3 for epoxy novolac resin and the filler densities given in Table 2. The density of the hybrid filler was calculated according to the rule of mixture.

The characterization of the char residue of the laminates was studied with a thermogravimetric analyzer (TGA/STDA851e) from Mettler Toledo (Columbus). The samples (15–20 mg) were heated from 25°C to 900°C at a heating rate of 10 K/min under 50 mL/min nitrogen purge. The char yield was evaluated at 900°C .

Three-point bending test is carried out to find out the flexural properties of reinforced laminates (ASTM D-790-03 and DIN EN 178:2003). The cut samples were conditioned at $23 \pm 2^\circ\text{C}$ and $50 \pm 5\%$ r.h. for 48 h. Five specimens from each sample were measured and averaged. A force of 2 N was applied on all the specimens with a strain rate of 2 mm/min. The elastic modulus (E_f) and the flexural strength (σ_f) were obtained from each test.

RESULTS AND DISCUSSION

Laminate Quality

Areal Weights of Prepregs, Glass Transition Temperature, and Fiber Volume Content. The areal weights of the produced prepregs were kept constant with a deviation of $129 \pm 3.1\text{ g/m}^2$ or 2.4%, as the coating unit distance was kept constant, and therefore, the resin film thickness was the same only varying because of the different filler densities. The neat epoxy areal weight was taken as reference and compared with the other systems. The FVC was determined with two different methods. One route was via TGA and the calculation of mass fractions on the basis of the rule of mixture and the densities of each component. The FVC calculated via measured density of the laminates differentiates due to the fact that pore inclusions lead to lower density values as the sample might float. Table 2 shows that the FVC (TGA) is in the range of $9.5 \pm 1.5\text{ vol}\%$ and the filler contents have an average of $14.2 \pm 1.5\text{ vol}\%$. The resin content for the unfilled laminate is the highest with 91 vol%, whereas the filled laminate range between $75 \pm 3\text{ vol}\%$. This shows that the filled laminate can be correlated toward their final properties.

Table 3 summarizes the results of the measured glass transition temperature and FVC for all laminate systems. The glass transition temperature (T_g) is an important parameter and determines the maximum service temperature range for a given laminate system. As it can be seen below, the glass transition temperature of the neat laminate is 235°C . The addition of 2 and 12 μm BN only slightly increases the T_g to 236°C and 237°C , respectively.

Morphological Characterization

Filler Distribution, Orientation, and Network Formation. The dispersion and network morphology of the fillers in the laminates

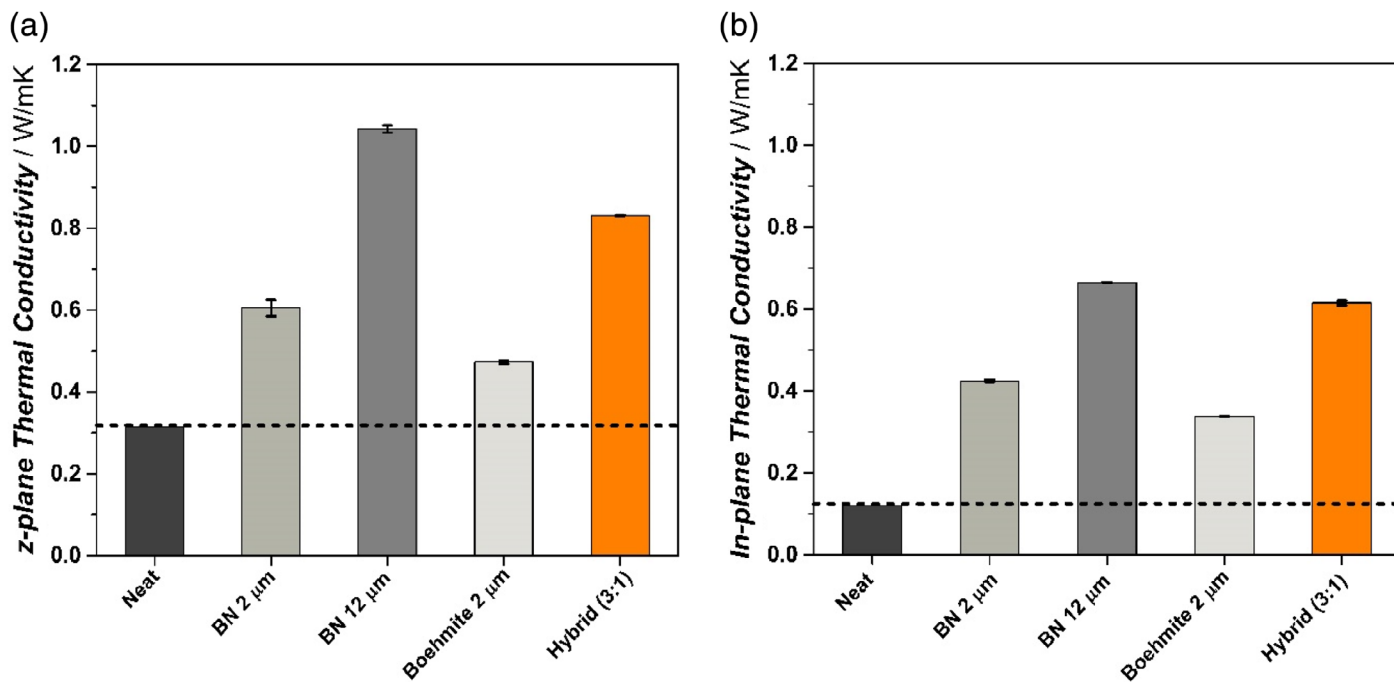


FIG. 4. (a) TC measured with THB in through-thickness (z -plane) and (b) in-plane (x/y -) direction of the chosen GFRP laminates. [Color figure can be viewed at wileyonlinelibrary.com]

was studied with SEM. The cross sections in $500\times$ and $1,000\times$ can be seen in Fig. 2. The first row of the micrographs (Fig. 2a and b) shows the unfilled laminate. The GF tows are fully impregnated with the resin matrix. In between the fabric, the resin rich-area (in dark gray) is visible. In general, the incorporation of the different fillers does not lead to any concentration gradient, that is, any filtration along the x/y -axis in between the different prepreg layers although the resin viscosity is at a minimum during the curing stage. The fillers are entrapped at their positions uniformly and the resin flows through the intertow regions. The incorporation of 20 vol% 2- μm -sized Boehmite particles (Fig. 2c and d) shows that the resin-rich area is now covered with the particles. These particles are well dispersed with only very few agglomerates. The orientation of these fillers is random. However, these particles infiltrate the single GF tows but also the intratow region homogeneously (Fig. 2e and f). The low thermally conductive GF barrier therefore is bridged with the Boehmite particles. The 2- μm -sized BN platelets are also well dispersed without any agglomeration formation. However, their thermal network is not as built up as compared with the microstructure formed by the

Boehmite particles. The larger BN 12- μm (Fig. 2g and h) platelets show an obvious thermal pathway, especially in the intertow region. Their orientation is anisotropic and the top edges of each particle are in close contact to each other. *Per contra*, the intratow regions are not infiltrated as the aspect ratio is too high. The particles are rather filtered at the outer corners of these GF fibers, and orientate themselves horizontally with some particles being broken. In addition, the area close to the edge of the tow shows a concentration gradient, meaning there are fewer fillers located

TABLE 5. TC and corresponding heating/cooling rates of the filled epoxy novolac laminates.

Specimen type	Thermal conductivity (W/m K)	Heating rate ($^{\circ}\text{C}/\text{min}$)	Cooling rate ($^{\circ}\text{C}/\text{min}$)
Neat EP novolac	0.181	0.6177	0.2450
EP + BN 2 μm	0.426	0.6787	0.3124
EP + BN 12 μm	0.545	0.6837	0.2879
EP + BT 2 μm	0.359	0.6248	0.3331
Hybrid	0.560	0.6904	0.3088

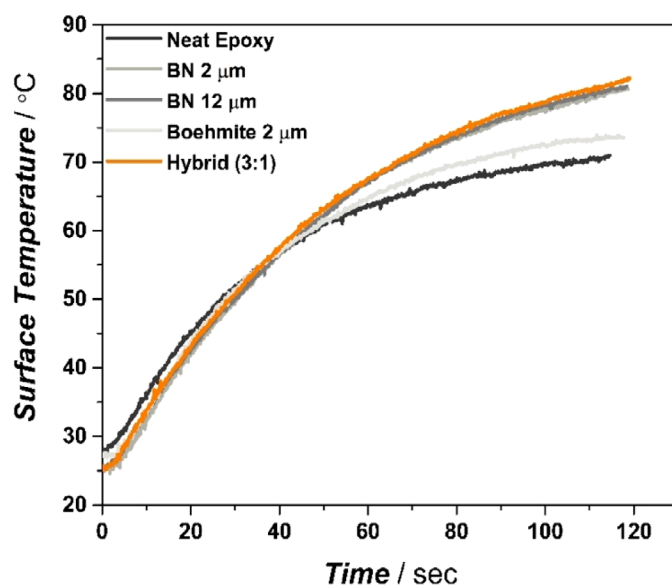


FIG. 5. Heating rates of the GFRP laminates recorded with IR-thermal imaging indicating the higher heat absorption and transfer behavior for the filled systems. [Color figure can be viewed at wileyonlinelibrary.com]

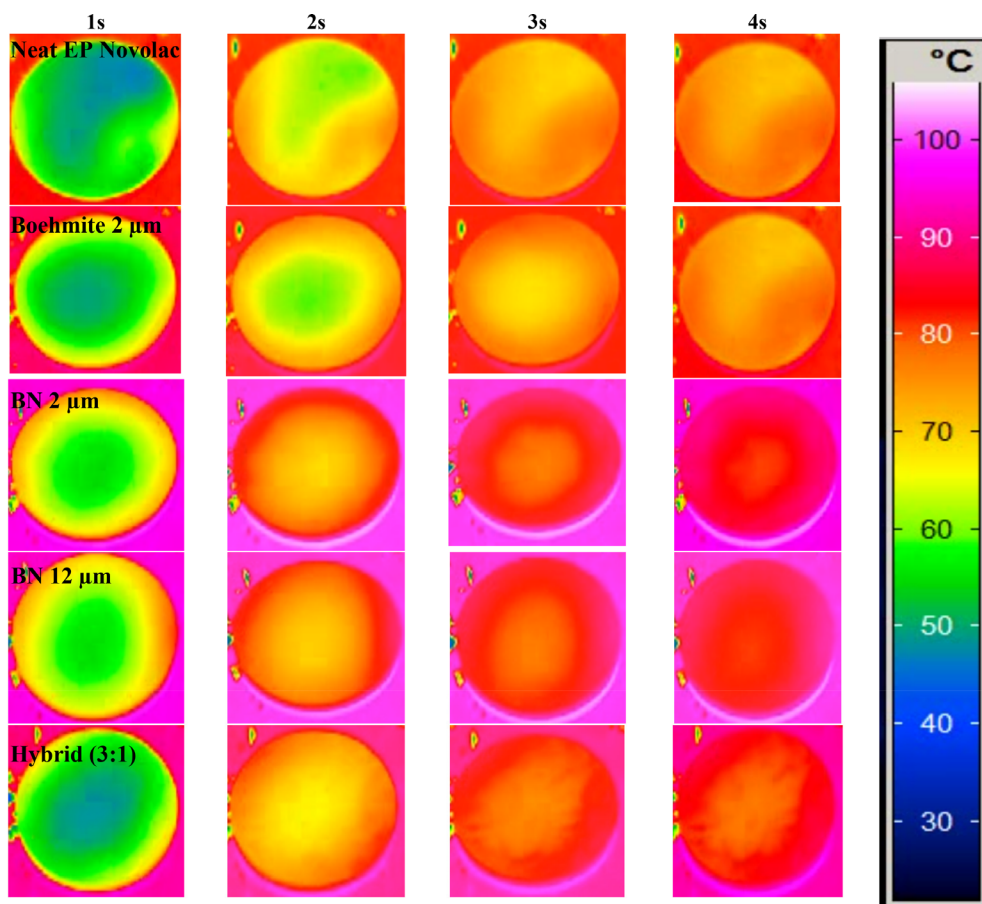


FIG. 6. IR images taken at the first 4 s for each system indicating the different heating stages which are according to their intrinsic TC. [Color figure can be viewed at wileyonlinelibrary.com]

there. Finally, the combination of BT 2 μm and BN 12 μm (Fig. 2i and j) shows a combinational effect in regard to the microstructure and the filler network. The larger BN platelets fill the area between the intertows in anisotropic orientation. The smaller particles fill the free gaps between the BN platelets. The packing density therefore reaches its maximum. Furthermore, the small Boehmite particles, as already observed in the unimodal laminate, infiltrate the intratow region and help form a continuous network throughout the z -plane.

Thermal and Flame-Retardant Properties

Characterization of the through-Thickness Thermal Conductivity. The TC value was measured in the *through*-plane (z -plane) of polished laminate samples via a heat flow meter. In Fig. 3, the measured TC values for the highly filled GFRP laminate

systems can be seen. The TC value for GF-reinforced neat epoxy novolac is 0.18 W/mK. This value is comparable with the commercially available FR-4 (0.3–0.4 W/mK) [25] value and also according to the neat epoxy novolac without GF reinforcement (0.20 W/mK). The slight deviation might arise due to scattering effects or due to the inclusion of air voids that lowers the heat transfer. The TC of E-glass is known to be between 0.9 and 1.35 W/mK, depending on the measuring method [26]. Adding 20 vol% 2- μm Boehmite particles (AOH EXS) increases the TC from 0.181 to 0.359 W/mK. Although the z -plane TC of Boehmite is known to be approximately 30 W/mK in literature, the increment in TC is still about 98% compared with the neat epoxy laminate. Such an increase can be attributed to the good dispersion and random orientation of the Boehmite particles, resulting in a dense filler network in the laminate (Fig. 2c and d). The addition of 20 vol% 2- μm boron nitride (BN 2 μm) exhibits a z -plane TC value of 0.426 W/mK, which is a 136% increment compared with

TABLE 6. Combustion and flame-retardant behavior comparison of the filled EP novolac laminates (heat flux of 35 kW/m²).

Composition	t_{ig} (s)	Residual weight (wt%)	PHRR (kW/m ²)	THE (MJ/m ²)	TSR (m ² /m ²)	(THE/ML)/ MJ/ g ²	FIGRA (kW/m ² s)
Neat EP novolac	88	40.80	686.3	48.4	1850	2.55	6.5
EP + BN 2 μm	135	56.32	588.1	51.4	2028	2.53	4.0
EP + BN 12 μm	130	57.81	655.6	49.4	1919	2.38	4.0
EP + BT 2 μm	111	55.02	383.9	49.5	1,656	2.43	2.6
Hybrid	136	54.67	593.2	48.0	1870	2.22	3.3

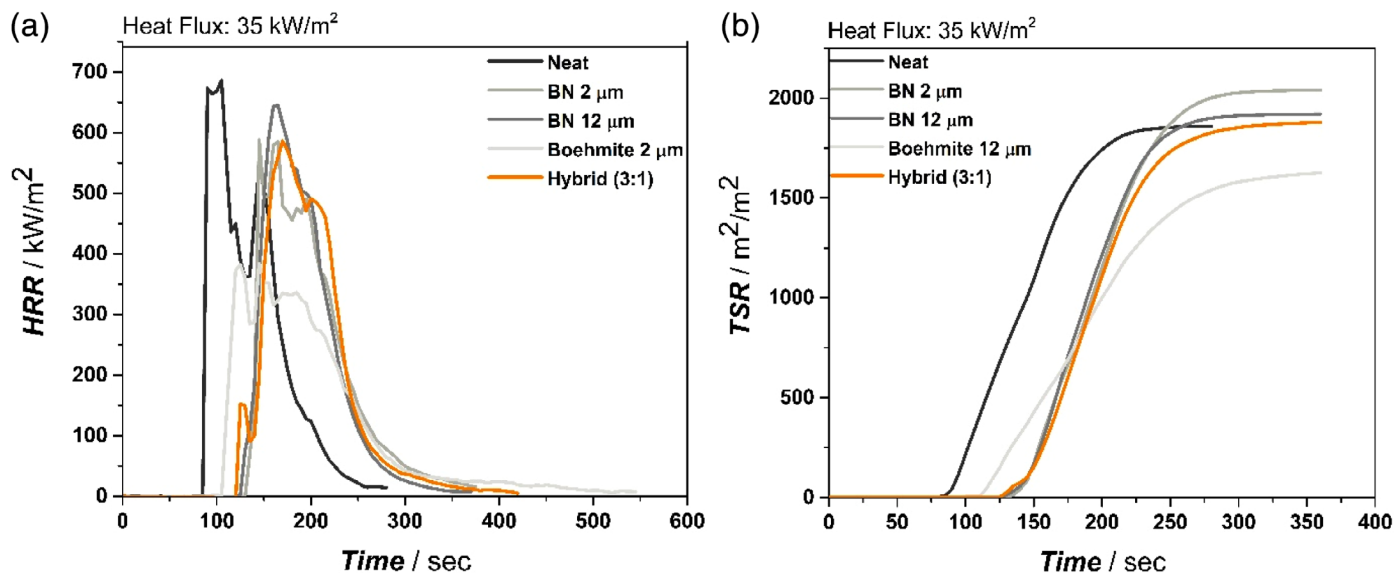


FIG. 7. (a) HRR in dependency of time curves and (b) the corresponding TSR rate in dependency of time for different laminate systems measured at applied 35 kW/m² heat flux in a cone calorimeter. [Color figure can be viewed at wileyonlinelibrary.com]

the reference neat epoxy novolac. Moreover, the 12-μm boron nitride (BN 12 μm) exhibits a TC value of 0.545 W/mK. This implies that increasing the lateral platelet size and aspect ratio of *h*-BN has a positive impact on the TC. The filler arrangement of the 12 μm BN platelets in the SEM micrographs shows that these platelets randomly orientate only with their filler edges touching. The BN 2 μm filler is well dispersed without any agglomeration formation; however, the interfiller distance is too high, and therefore, the resin matrix acts as a thermal barrier (Fig. 2e and f). The highest TC was achieved with the hybrid filled laminate (0.560 W/mK). The hybrid laminate, the 12 μm BN platelets, and the 2 μm Boehmite particles are mixed in the ratio of 3 to 1, respectively. Thus, it is interesting to see that the partial replacement of 12 μm-BN with 2-μm Boehmite results in a TC value close to the unimodal filled BN 12-μm system. The SEM micrographs (Fig. 2i and j) show that the bigger BN platelets form a random conducting filler network and the smaller particles attach to the free gaps in between this network. More importantly, the insulating GF barrier is infiltrated by the fillers. The small Boehmite particles infiltrate the tight fiber bundle, whereas in the area with the loose fiber bundles, the BN 12 μm is more prominent. Therefore, the small particles act as links between the arranged bigger particles.

Characterization of the through- and in-plane-Thickness Thermal Conductivity. The *z*- and *x/y*-directions of the TC was determined using the THB sensor. This comparison was used as a confirmation of the random filler distribution as platelet-shaped fillers such as BN exhibit a much higher TC in the *x/y*-plane (300 W/mK) rather

than in the *z*-plane (30 W/mK). From the direct comparison of the values obtained in the *z*-direction (heat flow meter vs. THB in Table 4), it is observed that the values obtained with the THB are higher. One reason might be that this measurement gives absolute values without uncertainty leaving behind. As seen in Fig. 4, the *z*-plane TC of the neat Epoxy laminate is 0.314 W/mK, which is considerably higher than the 0.181 W/mK obtained from the hot plate method. This implies that the E-glass reinforcement is slightly thermally conductive although the interpreg distance, the resin-rich area between the glass-fiber bundles, is roughly 50 μm. However, the trend for the measured TC between both methods is the same: Boehmite 2 μm, BN 2 μm, and BN 12 μm resulting in values of 0.473, 0.605, and 1.043 W/mK, respectively (Table 4). The hybrid laminate has a TC of 0.831 W/mK, slightly lower than the unimodal filled BN 12 μm.

The measurement in the *x/y*-direction of the samples shows that the increment of TC roughly follows the same trend between the GFRP systems: neat Epoxy, Boehmite 2 μm, BN 2 μm, hybrid, and BN 12 μm. The Boehmite-filled laminate has the lowest deviation comparing the results of the two methods and between the two measuring directions.

Thus, a slight anisotropic effect of the Boron Nitride-filled systems is visible. The SEM micrographs show that the BN 12-μm platelets have a certain random orientation. However, only very few are orientated in the *x/y*-direction. The majority is slightly tilted or is orientated in the preferred *z*-plane resulting in a higher thermal heat transfer.

TABLE 7. EDX results of studied elements the tested samples.

Composition	B (K) (wt%)	C (K) (wt%)	N (K) (wt%)	O (K) (wt%)	Al (K) (wt%)	Si (K) (wt%)
Neat EP novolac	6	68	6	9	6	4
EP + BN 12 μm	15	2.3	80	1.7	—	1
EP + BT 2 μm	5	16	3	50	25	2
Hybrid	10	7	26	33	17	5

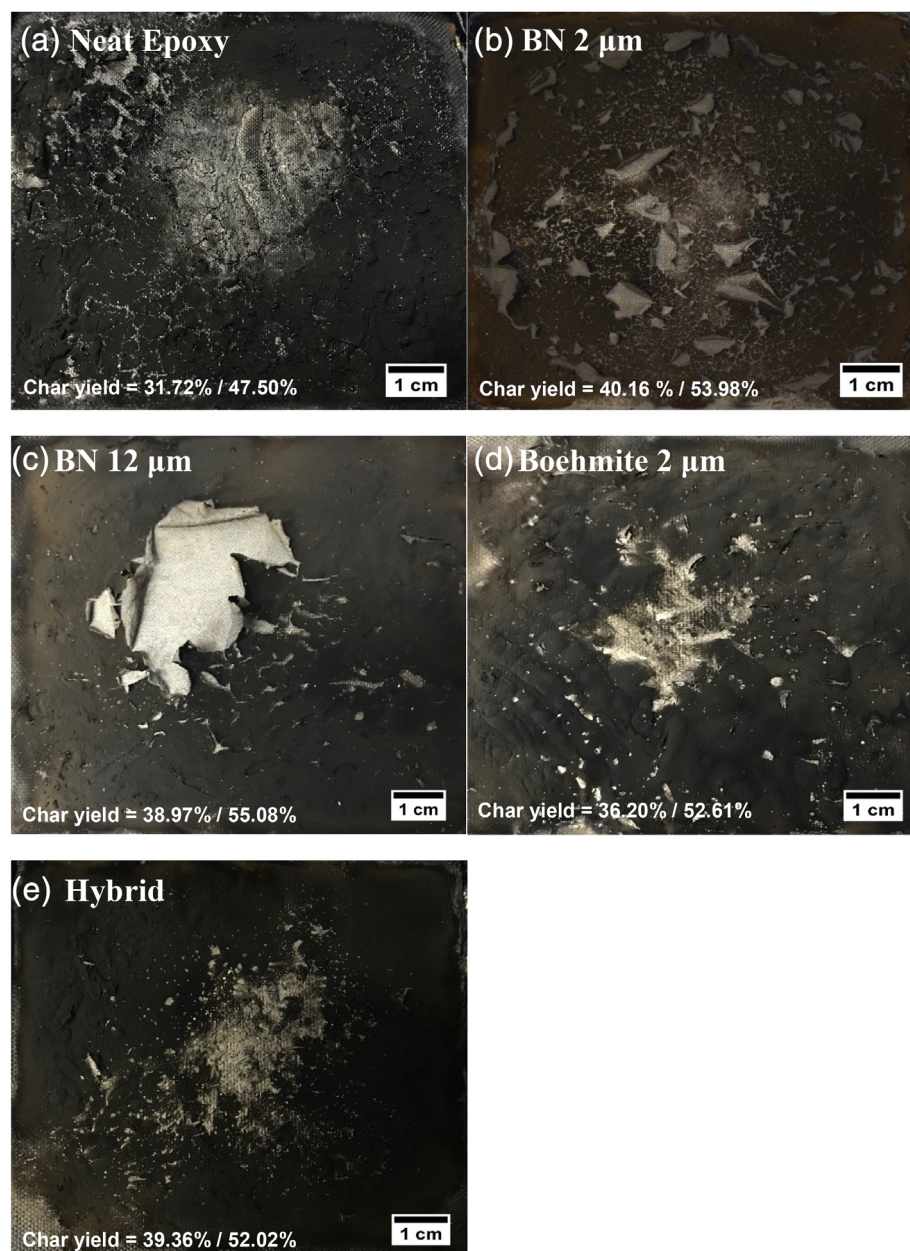


FIG. 8. Top-view photographs of the char residues captured after the cone calorimetry tests at a heat flux of 35 kW/m^2 for the unimodal and hybrid-filled GFRP laminates. The char yield was studied with TGA in air (left value) and in inert (N_2) (right value) conditions. The photographs indicate the different char thickness and cracking behavior, a) neat, b) BN $2 \mu\text{m}$, c) BN $12 \mu\text{m}$, d) Boehmite $2 \mu\text{m}$ and e) Hybrid laminate. [Color figure can be viewed at wileyonlinelibrary.com]

Thermography Imaging. Thermal imaging cameras are ideal tools to use in mapping out the heat patterns in electronic components. It is a known fact that when some electric current passes through a circuit board, heat is generated due to the *Joule effect*. Especially after miniaturization trend of electronics, the overall performance load on a circuit board has exceptionally increased. The generated heat during use can be as high as 165°C [27].

Table 5 shows the summarized results of the measured z -plane TC in comparison with the heating/cooling rates observed with the thermal imaging camera of the laminates.

The heating profiles of different highly filled GFRP laminates, the hybrid, and the unimodal BN $12 \mu\text{m}$ laminates show the highest and fastest increase in temperature (Fig. 5). The neat

epoxy laminate attains the lowest temperature increase. Only after 2 min, it was observed that the initial temperature of the best systems was reached. The unimodal Boehmite laminate exhibits slightly higher heating rate than the neat epoxy. In general, the nonlinear heating/cooling profiles (temperature = f [time]) match the trend accordingly with the measured TC. The faster a sample heats up, the faster it should cool down as well.

The infrared (IR) images can be seen in Fig. 6. Each sample was recorded for a total of 2 min. However, the first few seconds are most important as there the heat absorption and heat transfer (when cooling) are explicitly shown the best way. The neat epoxy novolac laminate shows an uneven heat distribution within the sample diameter indicating that the heat absorption, that is, the

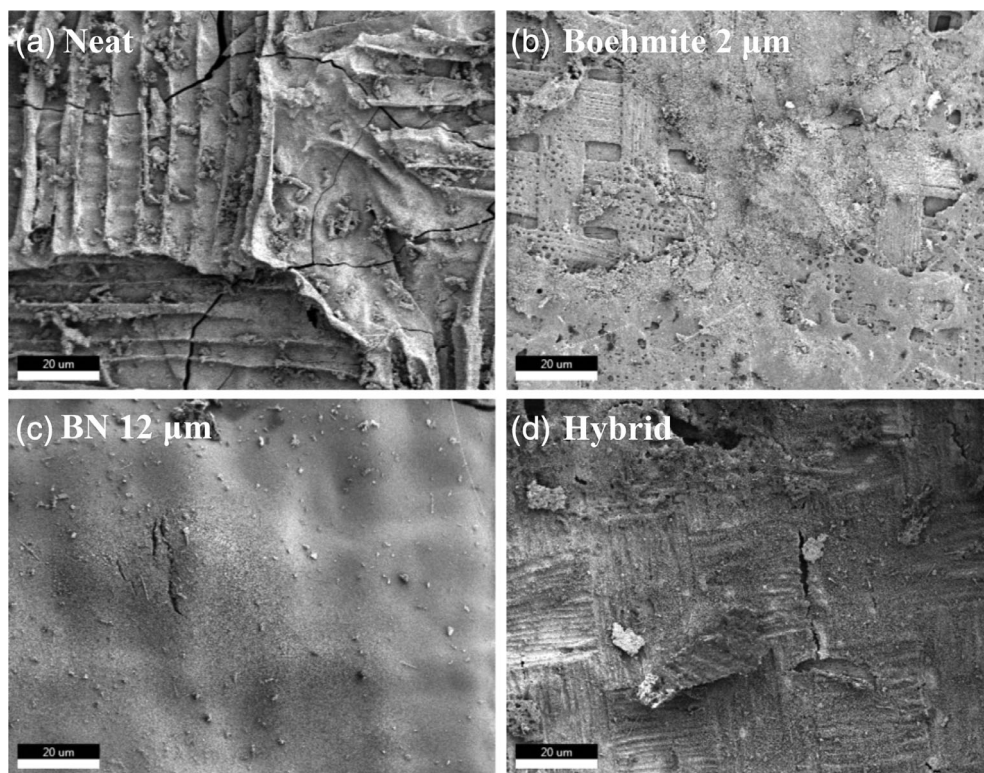


FIG. 9. SEM spectra of the burnt GFRP samples showing the char morphology (magnification of 250 x). The corresponding elemental composition on the presence of C, O, N, Al, Si and B of the char residues was studied for the a) neat, b) Boehmite 2 μm , c) BN 12 μm and d) Hybrid laminate.

thermal conductivity is low. With the addition of Boehmite, with a slightly higher TC property, the heat absorption is more even from the sample corner to the sample middle part. The two BN-filled laminates have the highest TC, and therefore have the quickest thermal absorption. The size effect is only slightly indicated when comparing the images after 4 s heat exposure. The BN 12 μm -platelets show the highest temperature measured within the lowest time frame. The combination of BN and Boehmite in the hybrid laminate also shows a comparative heating rate very close to the value of BN 12 μm in unimodal use.

Characterization of the Flame-Retardant Effect via Cone Calorimetry

Cone calorimeter tests enable the evaluation of a forced combustion and access valuable information of the fire (retarding) behavior of materials. Table 6 and Fig. 7 show the results of the Cone Calorimetric test of the laminates. The neat, unfilled GF-laminate shows the shortest time to ignition (t_{ig}) and the highest PHRR resulting in the highest FIGRA value. This can be directly correlated with the high resin content of this laminate, which is approximately 15 vol% higher than the filled laminates.

TABLE 8. Results obtained from the three-point bending test.

Specimen type	E_f (GPa)	σ_f (GPa)	δ_f (%)
Neat EP novolac	6.69 ± 0.56	0.170 ± 0.093	2.3 ± 0.180
EP + BN 2 μm	8.15 ± 0.20	0.155 ± 0.050	2.0 ± 0.074
EP + BN 12 μm	9.27 ± 0.57	0.181 ± 0.115	2.5 ± 0.300
EP + BT 2 μm	8.89 ± 0.74	0.141 ± 0.115	1.5 ± 0.060
Hybrid	8.33 ± 0.60	0.166 ± 0.010	2.3 ± 0.160

With the partial incorporation of Boehmite and, therefore, lowering the resin content, the t_{ig} is slightly increased but the PHRR is lowered. Boehmite is stable up to 350°C and then decomposes in a two-step reaction to Al_2O_3 barrier on top of the burning sample. The addition of BN only increases the t_{ig} even further, due to its intrinsic ability of a better thermal transport, that is, the higher intrinsic TC and higher thermal stability (>1,200°C). However, the PHRR is rather comparable with the neat laminate. The size of the BN platelets shows that the smaller BN is more efficient.

The combination of both fillers, Boehmite and BN 12 μm , respectively, results in the highest T_{ig} and highest t (PHRR) indicating a combinational effect of increasing the t_{ig} and lowering the PHRR. The total heat evolved (THE) is the highest for the BN 2- μm -filled laminate and the lowest when combining the two fillers, BN and Boehmite in the hybrid system indicating a synergistic effect. The smoke production rate (TSR) (Table 6 and Fig. 7b) is an important parameter when discussing fire hazardous materials as smoke production usually starts when the material is ignited. The HRR and TSR (Fig. 7a and b) are lowest for Boehmite, which is the only FR filler used. The aluminum oxide layer that is formed on the surface (also see EDX results in Table 7) suppresses the exchange between ambient air and also the release of volatiles. Boehmite also shows a higher effective heat of combustion values (THE/ML) indicating higher activity in the gas phase above the burning material.

Figure 8 shows the digital images obtained from the samples after the cone calorimetry testing (top-view perspective). The tested samples were further investigated with SEM/EDX (Fig. 9 and Table 7) in order to get more insight into the occurring FR mechanisms. The digital images show that with the GF

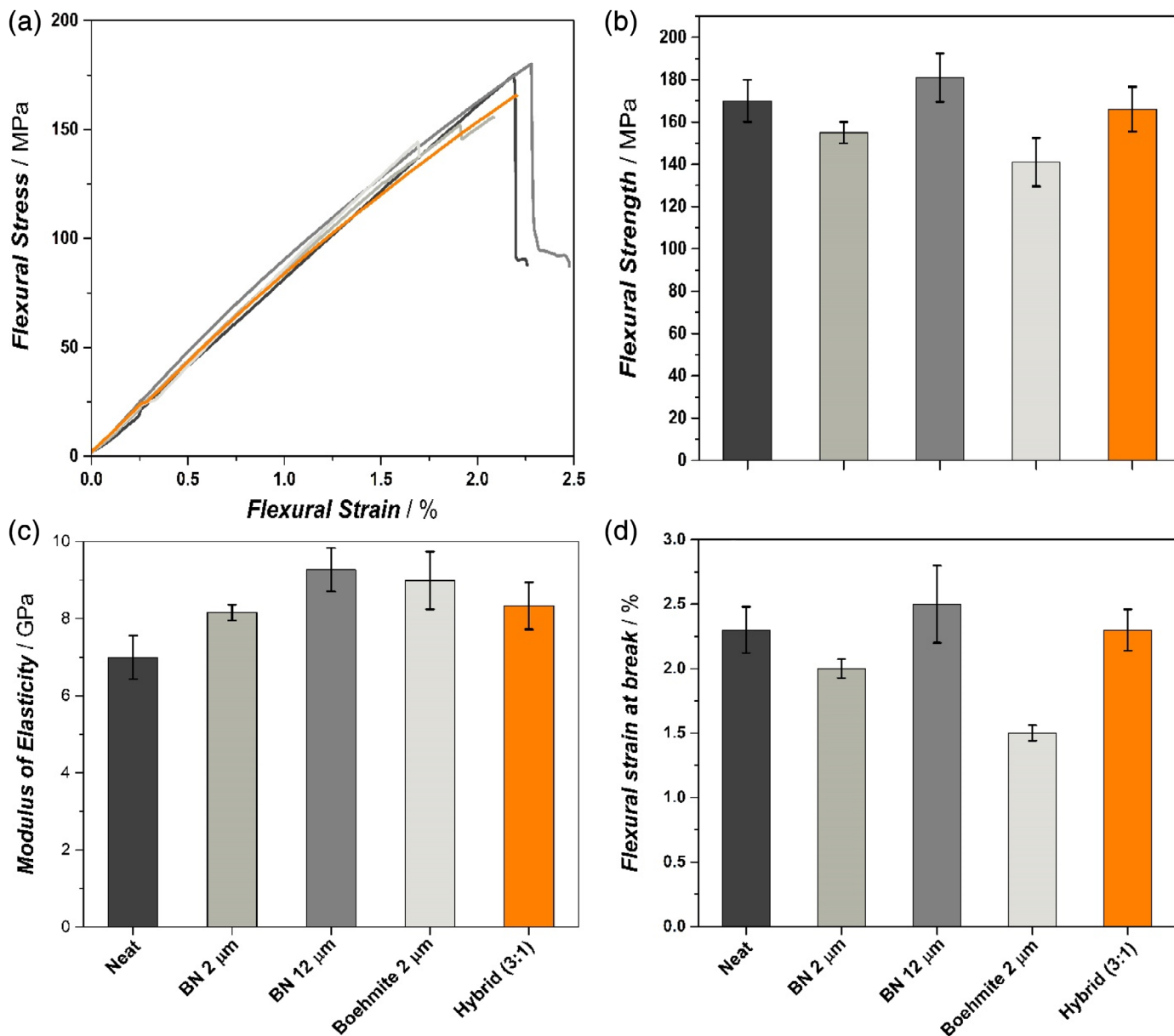


FIG. 10. (a) Flexural stress–strain curves, (b) flexural strength, (c) modulus of elasticity, and (d) flexural strain at break of the different laminates. [Color figure can be viewed at wileyonlinelibrary.com]

reinforcement, the structural stability is apparent, that is, no foaming or expansion in the z -axis is visible. The surface morphologies are very smooth with a continuous compact carbonaceous char on top (neat sample). With the addition of fillers, the char on top is more inherent and a change in color is visible indicating the formation of ceramic barriers. The char residue values examined with TGA in inert conditions shows that the incorporation of fillers leads to a higher charring effect than the neat material. In air conditions, the values are also higher for the filled laminates hinting a total degradation of polymeric material. The residue only consists of GF and filler material. The comparison of the char formation between TGA values and Cone Calorimeter shows that there is condensed-phase activity of the fillers (as explained in the “Introduction” section) [28].

The SEM spectra of the burned samples can be seen in Fig. 9. The EDX quantification was done scanning the surface of the samples (Table 7). The neat epoxy novolac sample is majorly

composed of carbon and oxygen. With the addition of Boehmite, the formation of a Al_2O_3 barrier is obvious with the major composition being O (K) and Al (K). The superficial carbon amount is very low, illustrating that the (degraded) polymer matrix is below the ceramic barrier, which therefore limits the oxidation of carbon to CO and CO_2 . This can also be related to the lowest TSR value of this system and its heat release during combustion. A formed char is linked to lowering these values [29]. The BN 12- μm sample is composed of B (K), N (K), O (K), and C (K). However, the carbon content compared with the Boehmite sample is very low. This demonstrates that the BN is not forming a compact superficial barrier releasing CO and CO_2 during polymer degradation, which is also in accordance with the second highest smoke release of all laminates. The hybrid-filled laminate SEM/EDX spectra reveal the occurrence of Al (K) and O (K) for the Boehmite component and B (K) and N (K) for the BN. The C (K) content is also very high.

In summary, the fire-specific indices (FIGRA, PHRR, t_{ig}) show that with the incorporation of fillers, a combinatoric effect can be achieved utilizing both fillers' positive aspects. This is also shown by the significant increase in t_{ig} by the addition of BN and the heat transfer inhibition by the shielding effect of the ceramic barrier formed by the decomposition of Boehmite. The char formation of the laminates indicates condensed-phase actions of the fillers. As a consequence, the combinations between BN and Boehmite suppress the volatile release and increase the materials' FR behavior.

Mechanical Characterization

Flexural Properties. GFRP laminates, used as base materials in PCBs are mostly subjected to cyclic and flexural stresses. Compared with metals, GFRP laminates are known to resist flexural stresses and fatigue, because the reinforcement and matrix phase in the laminates help absorb and transfer the forces. Moreover, the presence of GF as a reinforcement phase is known to take up more load and act as a "crack arrester," especially in the transverse direction. The flexural modulus values are seen in Table 8 and Fig. 10, which indicate that the modulus is highest for the 12- μ m-sized BN particles (9.27 GPa) and the lowest for the unfilled, neat laminate (6.69 GPa). BN 12 μ m exhibits a higher modulus than the BN 2- μ m laminates, which suggests that the higher aspect ratio fillers inhibit the crack propagation unless the applied bending forces are too high. BN 2- μ m fillers show lower E_f values than the BN 12 μ m laminates, which suggests that the higher interfacial area of these fillers have poor interaction with the resin matrix. Surface functionalization of the fillers could be a solution to improve the interfacial adhesion with the resin matrix. Boehmite has a higher E-modulus than the same size BN filler, 8.89 and 8.15 GPa, respectively. The hybrid laminate, however, shows the combinational effect of the two fillers. There is no clear synergistic effect visible.

CONCLUSIONS

In this study, highly filled epoxy novolac laminates were produced via a solvent-free impregnation production route. Although the filler concentration is high (20 vol% in the resin film), the fillers showed a good dispersion with no agglomerates formed. The fillers in each laminate system show a high degree of anisotropy and infiltration in GF tows, which suggests that the solvent-free processing route did not influence the filler orientation although the filler concentration is high. In addition, by adding BN and Boehmite simultaneously, the TC and FR properties were significantly improved. Compared with the TC of neat resin laminates (0.2 W/mK), values of 1.043 W/mK (*through-plane*) and 0.665 W/mK (*in-plane*) were obtained via THB for 20 vol % BN 12- μ m laminates. The hybrid laminates reached TC values of 0.831 W/mk (*through-plane*) and 0.615 W/mK (*in-plane*) as the smaller particles infiltrated the intratow region, while the larger particles are distributed in the intertow region, promoting the formation of conductive pathways. Boehmite-filled laminates showed suppressed HRR and TSR along with the lowest FIGRA value of 2.6, which was 60% lower than the neat laminate FIGRA value of 6.5. The combination of BN with Boehmite (ratio 3:1) hybrid laminates shows an FIGRA value of 3.3, which suggests that the behavior is combinatoric rather than synergistic. The modulus of elasticity for all filled systems showed better values than neat laminates, which suggests that the excellent dispersion of fillers across the resin matrix promotes crack inhibition. Future studies could be focused on surface functionalization of the fillers to further improve the thermal and fire-retardant properties.

ACKNOWLEDGMENTS

This work was financially supported by Federal Ministry of Economic Affairs and Energy (public funded project "Smart PVI Box", BMWi 0325916F). The authors also thank Nabaltec AG and OLIN Corp. for their material supply, G. Bakis for his support during the fruitful discussions, and J. Uhm for conducting Scanning Electron Microscopy (all from the Department of Polymer Engineering).

REFERENCES

1. D.M. Bigg, *Polym. Compos.*, **7**, 125 (1986). <https://doi.org/10.1002/pc.750070302>.
2. P. Bujard, *Intersoc. Conf. Therm. Phenom. Fabr. Oper. Electron. Components I-THERM'88*, 41 (1988). <https://doi.org/10.1109/ITHERM.1988.28676>.
3. M. Donnay, S. Tzavalas, and E. Logakis, *Compos. Sci. Technol.*, **110**, 152 (2015). <https://doi.org/10.1016/j.compscitech.2015.02.006>.
4. L. Huang, P. Zhu, G. Li, F. Zhou, D. Lu, R. Sun, and C. Wong, *J. Mater. Sci. Mater. Electron.*, **26**, 3564 (2015). <https://doi.org/10.1007/s10854-015-2870-1>.
5. F. Wang, X. Zeng, Y. Yao, R. Sun, J. Xu, and C.P. Wong, *Nat. Publ. Gr.*, **6**, 1 (2016). <https://doi.org/10.1038/srep19394>.
6. K. Gaska, A. Rybak, C. Kapusta, R. Sekula, and Artur Siwek, "A Study of Thermal Conductivity of Boron Nitride Epoxy Matrix Composites," in 15th European Conference on Composite Materials, 26th June (2012).
7. R. Kochetov, T. Andritsch, P.H.F. Morshuis, et al., *Annu. Rep. Conf. Electr. Insul. Dielectr. Phenom.*, 3 (2010). <https://doi.org/10.1109/CEIDP.2010.5723962>.
8. K.C. Yung, J. Wang, and T.M. Yue, *J. Compos. Mater.*, **42**, 2615 (2008). <https://doi.org/10.1177/0021998308096326>.
9. B.L. Zhu, J. Ma, J. Wu, et al., Study on the Properties of the Epoxy-Matrix Composites Filled with Thermally Conductive AlN and BN Ceramic Particles, (2010). doi:<https://doi.org/10.1002/app.32673>.
10. K. Kim, M. Kim, and J. Kim, *Compos. Sci. Technol.*, **103**, 72 (2014). <https://doi.org/10.1016/j.compscitech.2014.08.012>.
11. T. Wieme, D. Tang, L. Delva, D.R. D'hooge, and L. Cardon, *Polym. Eng. Sci.*, **58**, 466 (2018). <https://doi.org/10.1002/pen.24667>.
12. J.P. Hong, S.W. Yoon, T. Hwang, J.S. Oh, S.C. Hong, Y. Lee, and J.D. Nam, *Thermochim. Acta*, **537**, 70 (2012). <https://doi.org/10.1016/j.tca.2012.03.002>.
13. G. Zattini, S. Ballardini, T. Benelli, L. Mazzocchetti, and L. Giorgini, *Polym. Eng. Sci.*, 1 (2019). <https://doi.org/10.1002/pen.25121>.
14. E.S. Ogunniran, R. Sadiku, and S.S. Ray, *Macromol. Mater. Eng.*, **297**, 627 (2012). <https://doi.org/10.1002/mame.201100254>.
15. C. Yu, J. Zhang, Z. Li, W. Tian, L. Wang, J. Luo, Q. Li, X. Fan, and Y. Yao, *Compos. A Appl. Sci. Manuf.*, **98**, 25 (2017). <https://doi.org/10.1016/j.compositesa.2017.03.012>.
16. I. Tsekmes, R. Kochetov, P. Morshuis, et al., *IEEE Trans. Dielectr. Electr. Insul.*, **21**, 412 (2014). <https://doi.org/10.1109/TDEI.2013.004142>.
17. R. Kochetov, *Thermal and Electrical Properties of Nanocomposites, Including Material Processing*, Delft University of Technology, Delft, Netherlands (2012). ISBN: 9789462030343.
18. R.F. Hill and P.H. Supancic, *J. Am. Ceram. Soc.*, **85**, 851 (2002). <https://doi.org/10.1111/j.1151-2916.2002.tb00183.x>.

19. T. Hong, Y. Jung-Ho, and H. Sung-Woon, *Polym. Eng. Sci.*, **52**, 1 (2012). <https://doi.org/10.1002/pen.23190>.
20. J. Fu, L. Shi, and D. Zhang, *Polym. Eng. Sci.*, **50**, 1 (2010). <https://doi.org/10.1002/pen.21705>.
21. T.-Y. Tsai, S.-T. Lu, C.-J. Huang, and J.-X. Liu, *Polym. Eng. Sci.*, **48**, 1 (2008). <https://doi.org/10.1002/pen.20977>.
22. K. Devendra and T. Rangaswamy, *Mechanica Confab*, **2**, 39 (2013).
23. B. Fan, Y. Liu, D. He, and J. Bai, *Polymer (United Kingdom)*, **122**, 71 (2017). <https://doi.org/10.1016/j.polymer.2017.06.060>.
24. InfraTec GmbH Germany, IRBIS 3 Analysis Software. <https://www.infratec.eu/thermography/thermographic-software/irbis3/> (accessed May 21, 2019).
25. Product Data Sheet No. FR-406; Isola Corporation, 2018. <https://www.isola-group.com/wp-content/uploads/data-sheets/fr406.pdf>.
26. AZO Materials - E Glass Fibre Properties, AZoNetwork UK Ltd. <https://www.azom.com/properties.aspx?ArticleID=764> (accessed August 16, 2018).
27. D. Yang, , *Power Syst. Mag.* (2017). <https://www.pcbcart.com/article/content/automotive-pcb-design-considerations.html> (accessed June 2, 2019).
28. B. Schartel, B. Perret, B. Dittrich, M. Ciesielski, J. Krämer, P. Müller, V. Altstädt, L. Zang, and M. Döring, *Macromol. Mater. Eng.*, **301**, 9 (2016). <https://doi.org/10.1002/mame.201500250>.
29. J. Hausner, B. Fischer, M. Stöter, A. Edenharter, J. Schmid, R. Kunz, S. Rosenfeldt, V. Altstädt, and J. Breu, *Polym. Degrad. Stab.*, **128**, 141 (2016). <https://doi.org/10.1016/j.polymdegradstab.2016.03.015>.